Molecular and Dusty Layers of Asymptotic Giant Branch Stars Studied with the VLT Interferometer

Markus Wittkowski[1]
Iva Karovicova[1]
David A. Boboltz[2]
Eric Fossat[3]
Michael Ireland[4, 5]
Keiichi Ohnaka[6]
Michael Scholz[7, 8]
Francois van Wyk[9]
Patricia Whitelock[9, 10]
Peter R. Wood[11]
Albert A. Zijlstra[12]

[1] ESO
[2] United States Naval Observatory, Washington, DC, USA
[3] Laboratoire d'Université d'Astrophysique de Nice, France
[4] Dept. of Physics and Astronomy, Macquarie University, Sydney, Australia
[5] Australian Astronomical Observatory, Epping, Australia
[6] Max-Planck Institut für Radioastronomie, Bonn, Germany
[7] Zentrum für Astronomie, University of Heidelberg, Germany
[8] School of Physics, University of Sydney, Australia
[9] South African Astronomical Observatory, Cape Town, South Africa
[10] Astronomy Dept., University of Cape Town, Rondebusch, South Africa
[11] Australian National University, Canberra, Australia
[12] Jodrell Bank Centre for Astrophysics, University of Manchester, United Kingdom

Mass loss from asymptotic giant branch (AGB) stars is the most important driver for the evolution of low to intermediate mass stars towards planetary nebulae. It is also one of the most important sources of chemical enrichment of the interstellar medium. The mass-loss process originates in the extended atmosphere, whose structure is affected by stellar pulsations, and where molecular and dusty layers are formed. Optical interferometry resolves the extended atmospheres of AGB stars and thereby enables us to obtain measurements of the intensity profile across this region. We present an overview of recent results from our spectro-interferometric observations of AGB stars using the near- and mid-infrared instruments AMBER and MIDI of the VLT Interferometer.

Low to intermediate mass stars, including our Sun, evolve to red giant stars and subsequently to asymptotic giant branch stars after the hydrogen and helium supplies in the core have been exhausted by nuclear fusion. An AGB star is in the final stage of stellar evolution that is driven by nuclear fusion, where a degenerate carbon–oxygen core is surrounded by hydrogen- and helium-burning layers, a huge convective envelope and a very extended and diluted stellar atmosphere. Mass loss becomes increasingly important during AGB evolution, both for stellar evolution, and for the return of material to the interstellar medium. It reduces the convective stellar envelope until the star begins to shrink and evolves at constant luminosity toward the hotter post-AGB and planetary nebula (PN) phases, and is thus the most important driver for the further stellar evolution (e.g., Habing & Olofsson, 2003). Mass loss from AGB stars is also one of the most important sources for the chemical enrichment of the interstellar medium and of galaxies.

Depending on whether or not carbon has been dredged up from the core into the atmosphere, AGB stars appear in observations to have an oxygen-rich or a carbon-rich chemistry. A canonical model of the mass-loss process has been developed for the case of carbon-rich chemistry, where atmospheric carbon dust has a sufficiently large opacity to be radiatively accelerated and driven out of the gravitational potential of the star and where it drags the gas along. For the case of oxygen-rich chemistry, the details of this process are not understood, and are currently a matter of vigorous debate. Questions remain also for the carbon-rich case, such as regarding the formation of the recently detected oxygen-bearing molecule water in the inner atmospheres of carbon-rich AGB stars by the Herschel space mission (Decin et al., 2010).

AGB stars experience stellar pulsations, from semi-regular variable stars (SRVs) on the early AGB to large-amplitude long-period variable stars on the more evolved AGB, including Mira variables and more dust-enshrouded stars at the tip of the AGB. Pulsations and the induced shock fronts are expected to play a crucial role for the structure of the extended atmospheres, but the details of these processes and their effects on the mass-loss mechanism are also not well understood. Because of the extension of the atmosphere, temperatures are cool enough so that molecules form, leading to a scenario where molecular layers lie above the continuum-forming photosphere. Dust is formed and believed to be accelerated within this extended atmospheric region with a certain condensation sequence, where dust species of higher condensation temperatures form closer to the stellar surface and dust species with lower condensation temperatures form at larger distances. There is also a notion that different dust species may prevail at different stages along the AGB, along with increasing stellar luminosity and increasing mass-loss rate.

Optical interferometry at near-IR and mid-IR wavelengths has proved to be a powerful tool to study the extended atmosphere and dust condensation zones of AGB stars, because of its ability to spatially resolve these regions. Indeed, red giants and AGB stars have historically been prime targets for optical interferometry, because of their brightness and the match of their angular size to the typical spatial resolution of optical interferometers. However, despite the long history of such measurements, they still continue to provide important new constraints on the open questions discussed above. In particular, the near-infrared (NIR) instrument AMBER and the mid-infrared (MIR) instrument MIDI of the VLT Interferometer (VLTI) have been shown to be well suited for new measurements of AGB stars because of their unprecedented ability to provide *spectro*-interferometric observations with spectral resolutions of 35–12 000 (AMBER) and 30–230 (MIDI). Here, we report on very recent results (Karovicova et al., 2011; Wittkowski et al., 2011) from our ongoing programme to characterise molecular and dusty layers of AGB stars using the VLTI instruments.

Recent VLTI observations

VLTI observations of AGB stars using the instruments MIDI and AMBER started with the measurements described by Ohnaka et al. (2005) and Wittkowski et al. (2008), respectively. These studies

demonstrated that the spectro-interferometric capabilities of MIDI and AMBER are well suited to characterise the dusty and molecular layers of AGB stars.

We obtained MIDI data of the Mira variable AGB stars S Ori, GX Mon, RR Aql, R Cnc, and X Hya between 2004 and 2009. Some of these observations were aimed at performing a mid-infrared monitoring of AGB stars in order to investigate intracycle and cycle-to-cycle variability, and others were designed to complement AMBER observations to provide a more complete picture of the dusty *and* molecular layers at the same time. Mid-infrared interferometric monitoring of the sources listed above has been performed by Iva Karovicova during her PhD thesis, together with theoretical simulations of the expected variability. For example, the observations of RR Aql described in Karovicova et al. (2011) include 52 observations obtained at 13 epochs between April 2004 and July 2007 covering three pulsation cycles (Figure 1).

Using the AMBER instrument, we secured data of the Mira variables R Cnc, X Hya, W Vel, RW Vel, and RR Aql between 2008 and 2010 using the medium resolution mode with a spectral resolution of 1500. First results from these campaigns have been presented by Wittkowski et al. (2011).

Some of these observations were coordinated with concurrent VLBA observations of the SiO, H_2O, and OH maser emission (observation epochs shown in Figure 1), which provide complementary information on the kinematics and geometry of the molecular layers in which the maser emissions originate.

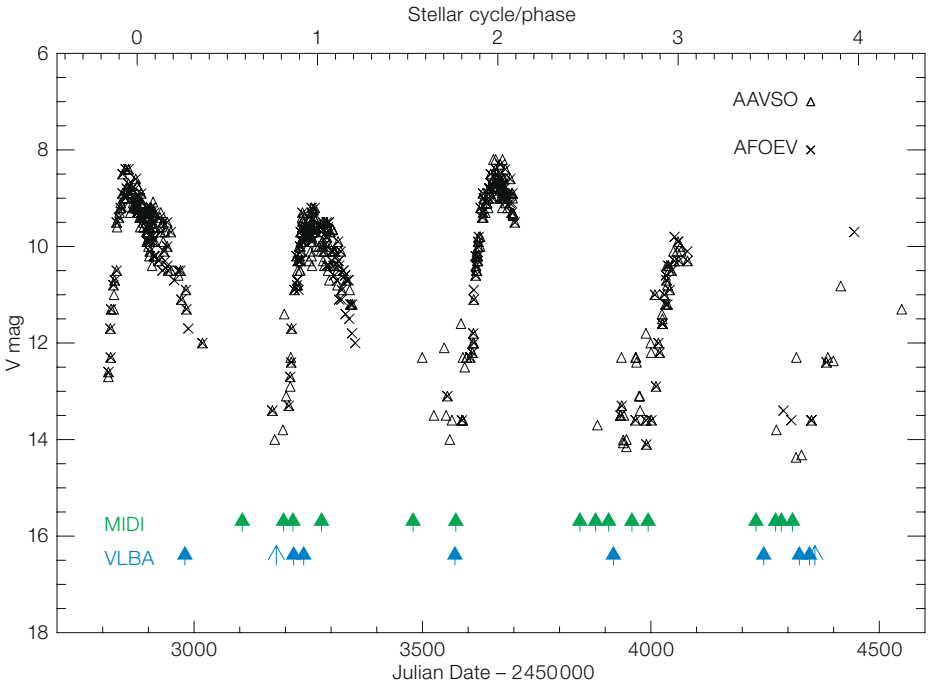

Figure 1. (Top) Visual light curve of RR Aql with our epochs of MIDI observations indicated in green. Epochs of Very Long Baseline Array (VLBA) observations are shown in blue. From Karovicova et al. (2011).

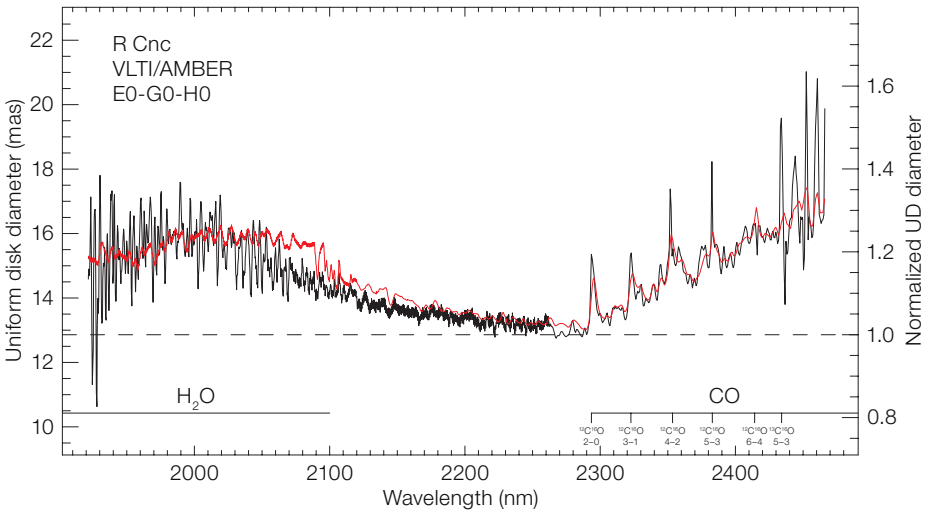

Figure 2. (Bottom) Uniform disc diameter as a function of wavelength obtained from VLTI/AMBER observations of the Mira variable AGB star R Cnc. The red line denotes the best-fit prediction from the recent dynamical atmosphere model series CODEX. From Wittkowski et al. (2011).

Structure of molecular layers

The medium resolution (R ~ 1500) near-infrared AMBER observations of the Mira variables of our sample confirmed a characteristic wavelength-dependent shape of the visibility function that is consistent with earlier low resolution AMBER observations of S Ori and that can be understood within the molecular layer scenario. In this scenario, the opacity of molecular layers, at NIR wavelengths, most importantly H_2O and CO, is larger at certain wavelengths so that the source appears larger and the visibility smaller, and lower at other wavelengths so that the source appears smaller and the visibility larger. Our observations confirm this effect, which has previously been detected by interferometric observations using a few narrowband filters. Hereby, the AMBER instrument has shown to be particularly well suited to further study and to quantification of this effect because of its wide wavelength coverage with high spectral resolution. In our measurements, the corresponding wavelength-dependent uniform disc (UD) diameters show a minimum near the near-continuum bandpass at 2.25 µm. They then increase by up to 30% toward the H_2O band at 2.0 µm and by up to

70% at the CO bandheads between 2.29 µm and 2.48 µm. Figure 2 shows the wavelength-dependent UD diameter for the example of the source R Cnc.

Recently, new dynamical model atmospheres for Mira variables were developed that are based on self-excited pulsation models and opacity-sampling radiation treatment (CODEX model series; Ireland et al., 2008; 2011), and which became available at the time of our data analysis. These models predict intensity profiles that are in excellent agreement with our visibility data and thus the uniform disc diameters, as also indicated in Figure 2. In order to estimate the effective temperatures of the sources at the time of our observations, we coordinated simultaneous near-infrared photometry at the South African Astronomical Observatory (SAAO). The effective temperature values obtained are consistent with those of the model atmospheres, as are the distances obtained from the radii and bolometric magnitudes. Altogether, the agreement of our observations with the CODEX model atmosphere series increases the confidence in the model approach, and thus in the scenario where the stratification of the extended atmosphere is largely determined by the pulsation that originates in the stellar interior and in which the molecular layers lie above the continuum-forming photosphere.

Inhomogeneities in molecular layers

The AMBER closure phase functions of our targets exhibit significant wavelength-dependent non-zero values at all wavelengths (Figure 3 shows the example of R Cnc). Non-zero values of the closure phase are indicative of deviations from point symmetry. Our data confirm non-zero closure phase data of Mira variables that have been previously observed by other interferometers. Again, the AMBER data provide additional information, thanks to their spectro-interferometric nature, that helps to constrain where within the atmosphere the asymmetric structure originates. In fact, we observe a complex wavelength-dependent closure phase signal that correlates with the features of the molecular layers, most importantly H_2O and CO. This indicates a complex non-spherical stratification of the extended atmosphere, where inhomogeneities are present at distances where molecules are formed and where molecular emission originates.

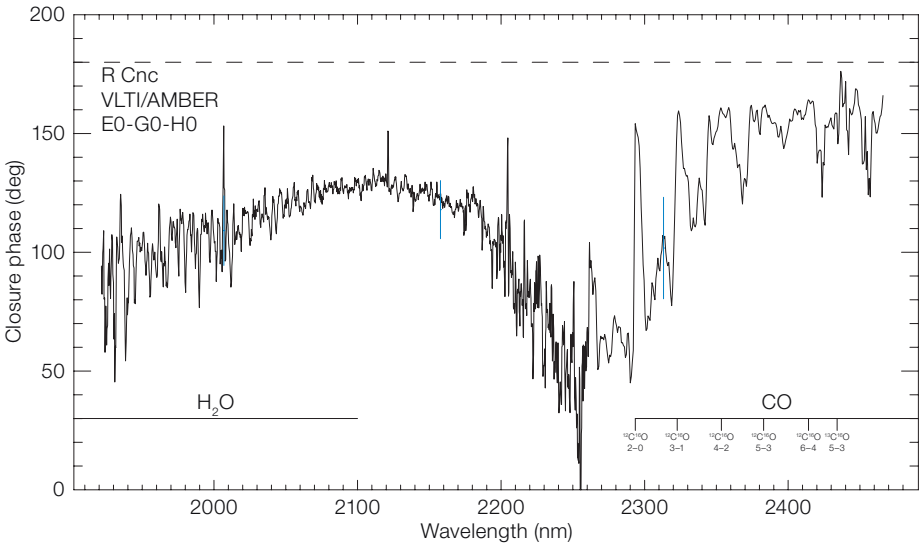

Figure 3. Closure phase as a function of wavelength for the example of the Mira variable AGB star R Cnc obtained with VLTI/AMBER. From Wittkowski et al. (2011).

With the limited amount of visibility data that we currently have, we cannot reconstruct the full morphology of the molecular layers. It would thus be important to conduct an interferometric imaging campaign of AGB stars at high spectral resolution. However, since the visibility data are overall well consistent with spherical models, we can already estimate that the deviation from point symmetry originates from substructure at a relatively low flux level for an overall spherical intensity distribution. For example, the values of R Cnc in the water vapour band shown in Figure 3 could be explained by an unresolved (up to 3 milliarcseconds [mas]) spot contributing 3% of the total flux at a separation of about 4 mas (for comparison, the photospheric diameter is estimated to 12 mas).

There are several physical mechanisms that may lead to asymmetric stellar surface structures. For our targets, we favour a scenario where the pulsation in the stellar interior induces chaotic motion in the outermost mass zones of the extended atmosphere that leads to different extensions of the mass zone on different sides of the star, and thus to the observed inhomogeneities. An inhomogeneous or clumpy molecular environment in the extended atmosphere may have important implications for the non-LTE chemistry in this region and may help to understand the formation of certain molecules such as water in carbon-rich AGB stars (Decin et al., 2010). It may also be the source of observed clumpy molecular features in the circumstellar environment at larger distances.

Variability of dusty layers

The observed MIDI visibility curves of RR Aql show significant wavelength dependence with a steep decrease from 8–~9.5 µm and a slow increase in the 9.5–13 µm range. The shape of the 8–13 µm flux spectrum with a maximum near 9.8 µm is known to be a characteristic silicate emission feature. Our rich sample of MIDI data of RR Aql cover pulsation phases between 0.45 and 0.85, i.e. minimum to pre-maximum phases, for a total of three cycles. For many different pulsation cycles and phases, we obtained data at similar projected baseline lengths and position angles. This gives us a unique opportunity to perform a meaningful direct comparison of interferometric data obtained at different pulsation phases and cycles. An example of such a direct visibility comparison is shown in Figure 4.

We concluded that our data do not show any evidence of intracycle or cycle-to-

cycle visibility variations within the probed range of pulsation phases (~ 0.45–0.85) and within our visibility accuracies of about 5–20%. This implies either that the mid-infrared sizes of the molecular and dusty layers of RR Aql do not significantly vary within our phase coverage or that the conducted observations are not sensitive enough to detect such variations. The MIDI photometry exhibits a 1–2σ signature of intracycle and cycle-to-cycle flux variations which are most pronounced toward the silicate emission feature at 9.8 μm. Additional observations with a dedicated mid-infrared spectrograph, such as the instrument VISIR at the VLT, are recommended to confirm the flux variations.

We performed a number of model simulations in order to investigate the visibility and photometry variations that are theoretically expected in the 8–13 μm wavelength range for the typical parameters of RR Aql. We used a radiative transfer model of the dust shell where the central source is described by the dust-free dynamic model atmosphere series, as they were used to model the near-IR AMBER data. We varied model parameters such as the phase of the central atmosphere model and the opacity and inner radius of the dust shell to investigate the expected photometry and visibility variations during a pulsation cycle. An example of such a simulation is shown in Figure 5.

These model simulations show that visibility variations are indeed not expected for the parameters and observational settings of RR Aql at wavelengths of 8–13 μm within the uncertainties of our observations. Variations in the flux spectra may in some cases just be detectable. Thus, our observational result of a constant visibility curve and only slightly varying flux spectra at wavelengths of 8–13 μm are consistent with, and not contradicting, theoretical expectations of a pulsating atmosphere. We used our simulations as well to determine the best baseline configurations for the parameters of certain targets in order to optimise future interferometric observing campaigns that aim at characterising the small expected visibility variations.

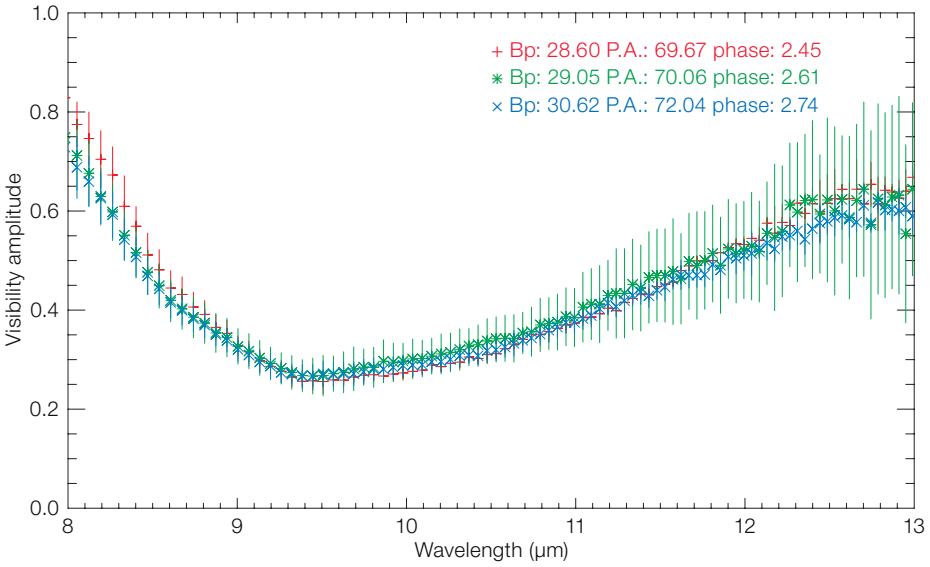

Figure 4. MIDI visibility amplitudes of RR Aql for different pulsation phases (indicated by different coloured points) within the same cycle, chosen to investigate intracycle visibility variations. From Karovicova et al. (2011).

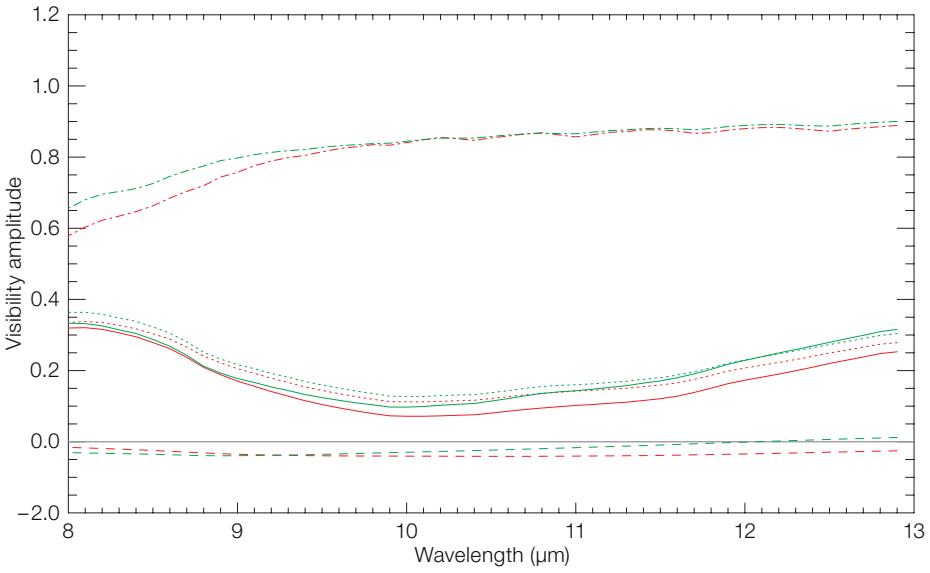

Figure 5. An example of expected intracycle visibility variation based on a simulation using two atmosphere models with a phase difference of 0.2 and a dust shell that is located closer to the star with a higher optical depth toward stellar minimum compared to stellar maximum. The solid green and red lines denote the two global models of this simulation, the dash–dotted lines the unattenuated stellar contribution, the dotted lines the attenuated stellar contribution and the dashed lines the dust shell contribution. From Karovicova et al. (2011).

Characteristics of dusty layers

We characterised RR Aql's dust shell by using radiative transfer models of shells of Al_2O_3 and/or silicate grains with independent inner radii and opacities, following earlier such attempts in the literature. We obtained best-fit results for RR Aql with a silicate shell alone. The addition of an Al_2O_3 shell did not result in any improvement in the model fits. The best-fit model for our average pulsation phase of $\Phi_V = 0.64 \pm 0.15$ includes a silicate dust shell with an optical depth of $\tau_V = 2.8 \pm 0.8$ and an inner radius of $R_{in} = 4.1 \pm 0.7\ R_{Phot}$ (where R_{Phot} is the photospheric radius) and uses a central intensity profile corresponding to an atmosphere model with an effective temperature of 2550 K. Figure 6 shows a comparison of our radiative transfer model to the RR Aql visibility data of one of our epochs. We conclude that a radiative transfer model of the circumstellar dust shell that uses dynamical model atmospheres representing the central stellar source can reproduce well the spectral shape of both the visibility and the photometry data (not shown).

In addition to RR Aql, we determined best-fit dust shell parameters for other sources of our sample (S Ori, GX Mon, and R Cnc). The mid-IR visibility and spectra of each star can be described by an Al_2O_3 dust shell with a typical inner radius of 2–2.5 stellar radii and/or a silicate dust shell with a typical inner radius of 4–5 stellar radii. This result is consistent with the scenario of a dust condensation sequence where Al_2O_3 grains form closer to the stellar surface and silicate grains at larger radii, which is as well consistent with the condensation temperatures. Our best-fit values of the optical depths of the Al_2O_3 and silicate dust shells together with the mass loss rates adopted from the literature may confirm earlier suggestions of a sequence where the dust content of stars with low mass-loss rates is dominated by Al_2O_3 grains, while the dust content of stars with high mass-loss rates predominantly exhibit substantial amounts of silicates.

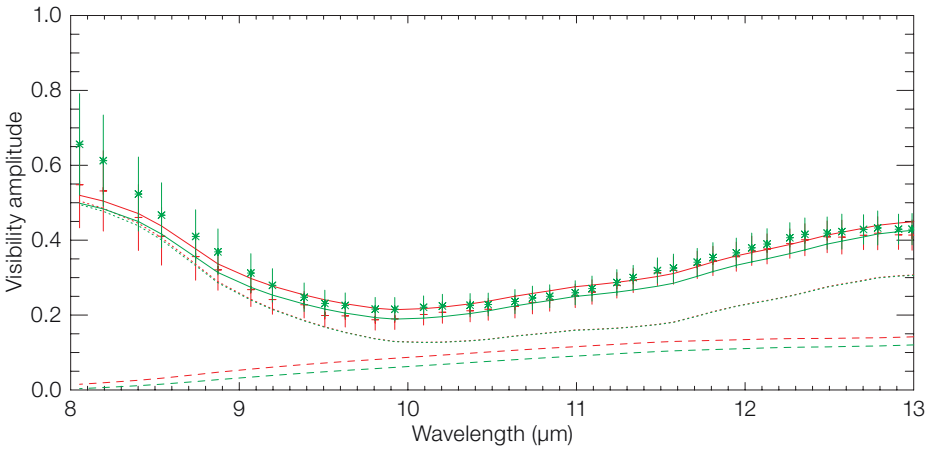

Figure 6. Radiative transfer model of RR Aql (solid lines) compared to the visibility data of one of our epochs including two observations. The solid lines indicate our best-fit model, while the contributions of the attenuated stellar and dust components alone are denoted by the dotted and dashed lines, respectively. From Karovicova et al. (2011).

References

Decin, L. et al. 2010, Nature, 467, 64
Habing, H. J & Olofsson, H. 2003, Astronomy and astrophysics library, New York, (Berlin: Springer)
Ireland, M. et al. 2008, MNRAS, 391, 1994
Ireland, M. et al. 2011, MNRAS, in press (arXiv 1107.3619)
Karovicova, I. et al. 2011, A&A, 532, A134
Ohnaka, K. et al. 2005, A&A, 429, 1057
Wittkowski, M. et al. 2008, A&A, 479, L21
Wittkowski, M. et al. 2011, A&A, 532, L7

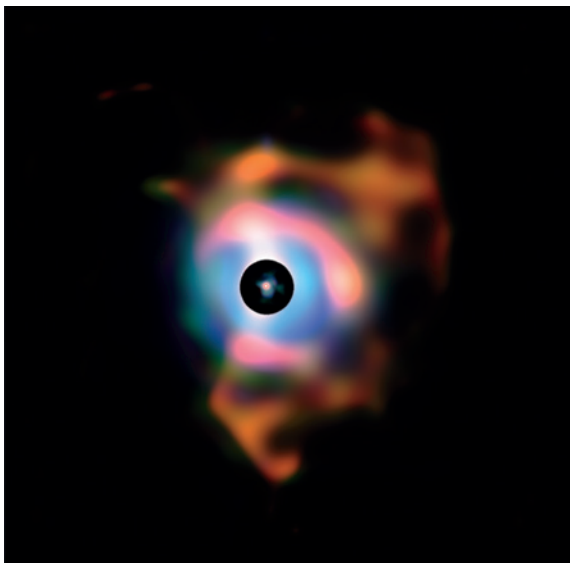

A composite of images from VISIR and NACO of the red supergiant star Betelgeuse. The image is 5.63 by 5.63 arcseconds in extent and shows the extension of the nebula around the star to be some 26 milli-parsec (550 AU). The supergiant star itself is resolved by interferometry at 44 milli-arcseconds (3.4 AU). The larger image is taken with VISIR in thermal-infrared filters sensitive to dust emission and the compact image (inside the occulting spot) is taken with NACO in *J*-, *H*- and *K*-band filters. Some of the non-spherically symmetric eruptions close to the star in the NACO image can be traced to much larger distances in the VISIR image. More details can be found in Kervella et al., A&A, 531, 117, 2011 and in Release eso1121.